INL/JOU-21-64062-Revision-0

Flow and arching of biomass particles in wedge-shaped hoppers

October 2021

Wencheng Jin, Jordan L Klinger, Yimin Lu, Sheng

Changing the World's Energy Future

INL/JOU-21-64062-Revision-0

Flow and arching of biomass particles in wedge-shaped hoppers

Wencheng Jin, Jordan L Klinger, Yimin Lu, Sheng

October 2021

Idaho National Laboratory
Idaho Falls, Idaho 83415

http://www.inl.gov

Prepared for the
U.S. Department of Energy
Under DOE Idaho Operations Office
Contract DE-AC07-05ID14517

Flow and arching of biomass particles in wedge-shaped hoppers

Yimin Lu,[†,‡] Wencheng Jin,[*,†] Jordan Klinger,[†] and Sheng Dai[‡]

†*Energy and Environment Science & Technology Directorate, Idaho National Laboratory, Idaho Falls, Idaho, 83415, USA*

‡*School of Civil and Environmental Engineering, Georgia Institute of Technology, Atlanta, GA, 30332, USA*

E-mail: Wencheng.Jin@inl.gov

Abstract

Poor understanding of the flow behavior of granular biomass material poses great challenges for the bioenergy industry, as the equipment functioning time is significantly reduced by handling issues like screw feeder clogging and hopper arching. In this work, the flow behavior of loblolly pine chips, including the mass flow rate and the critical outlet width, in a wedge-shaped hopper is investigated by combining physical experiments and numerical simulations. Comprehensive characterization of the flow response affected by the two material attributes (initial packing, particle density) and the three operational parameters (hopper outlet width, hopper inclination, and surcharge) is conducted. The results show that the hopper outlet width linearly controls the mass flow rate while the hopper inclination angle controls the critical outlet size. The packing determines whether the flow is smooth or surging, and the surcharge-induced compaction creates flow impedance. The magnitude of these influences varies from a slender hopper with a low inclination angle to a flat-bottom silo. These findings provide guidance for

hopper operation in the material handling industry and shed light on the construction of a novel design method for material handling equipment in biorefineries.

Keywords: biomass flowability, ground loblolly pine, hopper flow experiment, hopper arching, granular flow modeling

Introduction

Biomass has been considered as one of the most promising energy resources because of its nature abundance and easy access.[1–3] However, the commercialization of lignocellulosic biomass as an energy source has been substantially limited by its poor flowability, which often results in dramatic issues during bulk solids handling, for example, hopper arching, ratholing, and screw feeder jamming.[4–9] Fig. 1(a) demonstrates the wide application of hopper (marked with yellow boxes) in the transportation of biomass feedstock in a typical biorefinery, and Fig. 1(b) shows woody biomass material arching in a wedge-shaped hopper. The current operational reliability of a biorefinery is only 30%, which is far away from the goal 90% required by the U.S. Department of Energy to achieve the target cost of $3.00 per gallon of gasoline.[4,10]

The leading reason for these handling problems is the poor understanding of the granular biomass flow behavior. Comparing to conventional granular particles (e.g., sands), granular biomass particles have low particle density, high aspect ratio, high compressibility and high shear resistance. These unique characteristics, manifested through their porous microstructure and complex surface morphology, make the bulk flow behavior challenging to be characterized experimentally and theoretically.[11] In experiments, the standard characterization tests suffer from either a limited strain range to reach the critical shear state (e.g., tri-axial shear test) or inadequate measurement of full stress state (e.g., ring shear test) for granular biomass materials.[11–14] In theory, the classical constitutive models (e.g., Mohr-Coulomb, Drucker-Prager), proven to be able to capture the flow behavior of conventional granular materials, fail to represent the mechanical behavior of granular biomass

(a) Biomass material Process Development Unit (b) Arching in wedge-shaped hopper

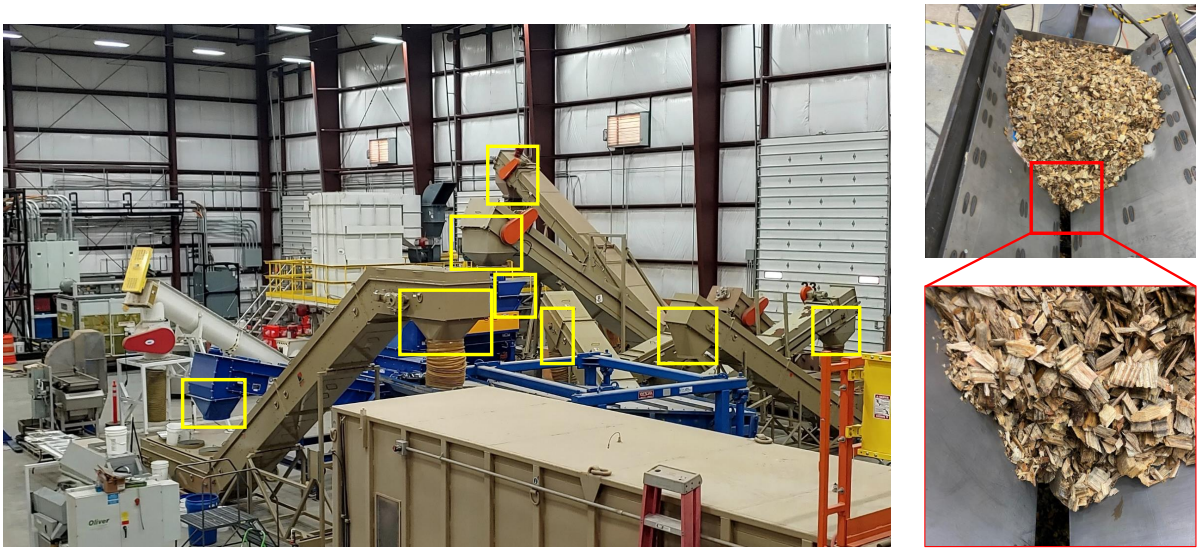

Figure 1: (a) A biomass material Process Development Unit at Idaho National Laboratory, Idaho Falls, ID, USA. Hoppers are marked out in the yellow boxes. (b) An example of woody biomass material arching in a wedge-shaped hopper.

materials.[15,16] Yet, the design of biomass material handling equipment still uses incompetent experimental methods and theoretical models, which results in material processing upsets in biorefineries. Take the most used material handling equipment, hopper/silo, as an example, its design is still guided by Jenike and colleagues' early work in the 1960s.[17–19] The design method has been experimentally and numerically demonstrated that it conservatively overestimates the critical outlet size of hopper/silo for various granular materials.[20–23] However, the hoppers/silos, designed by following this method, constantly experience arching/bridging in biorefineries, indicating the critical outlet width is underestimated.[13,24]

Hopper arching is a classical challenge in bulk solid handling, a significant amount of experimental and numerical studies have been conducted in literature. One of the focuses of these studies is the determination of the hopper critical outlet width for various materials (e.g., rocks, coals, ores, pharmaceutical particles, and ideal spherical beads).[22,25–27] Experimental characterization of a specific granular material is the most direct way to understand the flow behavior and quantify the critical outlet width. Yet, limited by the sensors on the hopper, experiments can only measure global flow response (e.g., flow rate, flow pattern),

cannot track the strain-stress behavior within the material. In addition, experiments at the industry-scale with a comprehensive test plan are not economically viable. Numerical simulations, with models validated by experiments, can address the experiment limitations listed above. For the hopper arching problem, both the Discrete Element Method (DEM) and the Continuum Mechanics-based Finite Element Method (FEM) have been utilized. DEM explicitly models the particle and has been proved suitable for investigating the granular interaction near the hopper outlet.[28,29] Yet, DEM is not capable of modeling the large-scale hopper flow due to its non-affordable computational cost even with the current supercomputing resources.[30,31] Without heavy computational burden, advanced FE Methods with a valid constitutive law have been successfully utilized to study the arching behavior in hoppers.[23,32] Most of these experimental and numerical studies focus on conventional granular materials (e.g., sands, pharmaceutical particles), and investigation on hopper arching for granular biomass material is missing.

To fill the knowledge gap on the flow behavior of biomass feedstock in a hopper, we combine physical experiments and numerical simulations in this study to understand the effect of the critical material attributes and the critical processing parameters on hopper flow. A customized hopper with adjustable inclination angle and outlet width is used for experimental investigation. The critical state theory-based hypoplastic model, calibrated and validated for ground loblolly pine,[11,15] is adopted as the constitutive law. Focused on flow performance in mass flow rate and hopper arching, we first present the development of a Coupled Eulerian-Lagrangian (CEL) FEM model with validation against the hopper flow experiment. Flow and arching affected by hopper inclination angle and opening size are investigated experimentally and numerically in the following. We then systematically analyze the influences of material packing, particle density, and hopper filling height or surcharge on flow performance. This study sets a foundation for the construction of a novel design method for flowing granular biomass material in a hopper.

Methods

Granular pine samples

The granular material used in this study is ground loblolly pine. The loblolly pine trees were grown on a southeastern Georgia plantation in the United States and harvested at a maturity of 24 years. The bark, limbs, and needles were removed with a flail chain debarker. The main bole of the tree was chipped at the plantation to a nominal 50 mm size, then hammer milled until the particles pass a retention screen of 6 mm. After the size-reduction processes, the granular pine chips were dried in a rotary drum and stored with a moisture content of approximately 6%. The particle size distribution (d_{10}=0.38 mm, d_{50}=0.82 mm, d_{90}=1.79 mm) is obtained by the sieve analysis and shown in Fig. 2(a) with a photo presenting the particle size and shape. Note that the dashed line is empirically extrapolated due to the lower limit of the sieve screen. Woody samples with a nominal particle size less than 2 mm is often considered in thermochemical conversion processes in biorefineries, and we denote this sample as *as-ground* in this study. A more detailed description of sample preparation has been reported in an earlier work.[15]

Experimental setup

A customized wedge-shaped hopper attached with a cuboid bin at the top, as shown in Fig. 2(b), was used to perform all the flow tests. Equipped with stepper motors, rack and pinion gearing on both sides, the hopper walls on both sides are capable of sliding as well as rotating through hand wheels and threaded supports at the top, which allow us to adjust hopper inclination and outlet size. The walls were synchronized and moved together to either a fixed position for measuring the discharge rate or were incrementally opened to measure the critical outlet width. Fig. 2(c) shows the 2D hopper geometry from the axial direction. The width of the bin is fixed as 0.6 m, and the length of the wall is adjustable by sliding

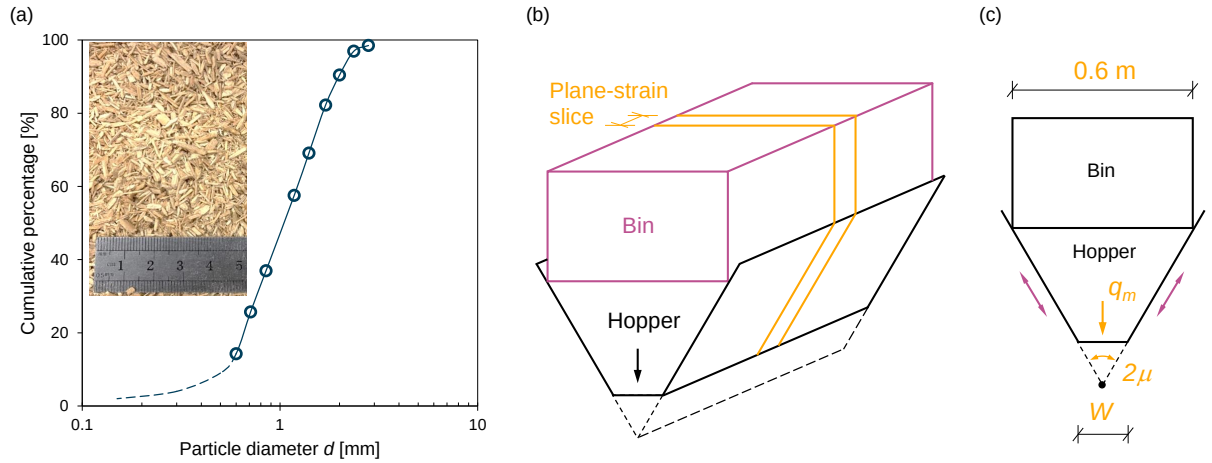

Figure 2: (a) Particle size distribution of the sample and a photograph presenting particle size and shape. The dashed line is empirically extrapolated due to the lower limit of the sieve screen to measure the particle size. (b) A schematic view of the experimental set-up: a wedge-shaped hopper extended with an upper cuboid bin. The numerical model is constructed using a slice with a finite thickness of 25 mm based on the plane strain condition. (c) The geometry and boundary conditions of the pseudo-3D numerical model. Note the outlet size is adjusted by sliding the hopper walls.

according to different hopper inclinations and outlet widths. We denote half of the angle between the two walls as the hopper inclination angle μ (Fig. 2(c)), and we use W to denote the hopper outlet width.

For each test, the hopper wall is adjusted to a specified inclination angle and is closed initially ($W = 0$). Granular biomass feedstock with a fixed mass M is loaded into the hopper and the bin. We initiate the flow test by sliding the wall until the hopper outlet reaches a preset opening width W. A balance with a readability of 5 g is placed below the outlet to measure the cumulative hopper discharging mass m_t against time. A typical $m_t - t$ response is shown in Fig. 3(a) as the yellow '$\times$'s. We calculate the mass flow rate q_m as the slope of the curve during the discharging period after eliminating the two ends of inception and decay.

In addition to quantifying the mass flow rate, we also measure the critical outlet width W_{cr}. Similar to the previous description, we first load the hopper with the biomass feedstock. Then, we open the outlet gate about 1 mm by sliding the wall and hold for 30 s to observe the

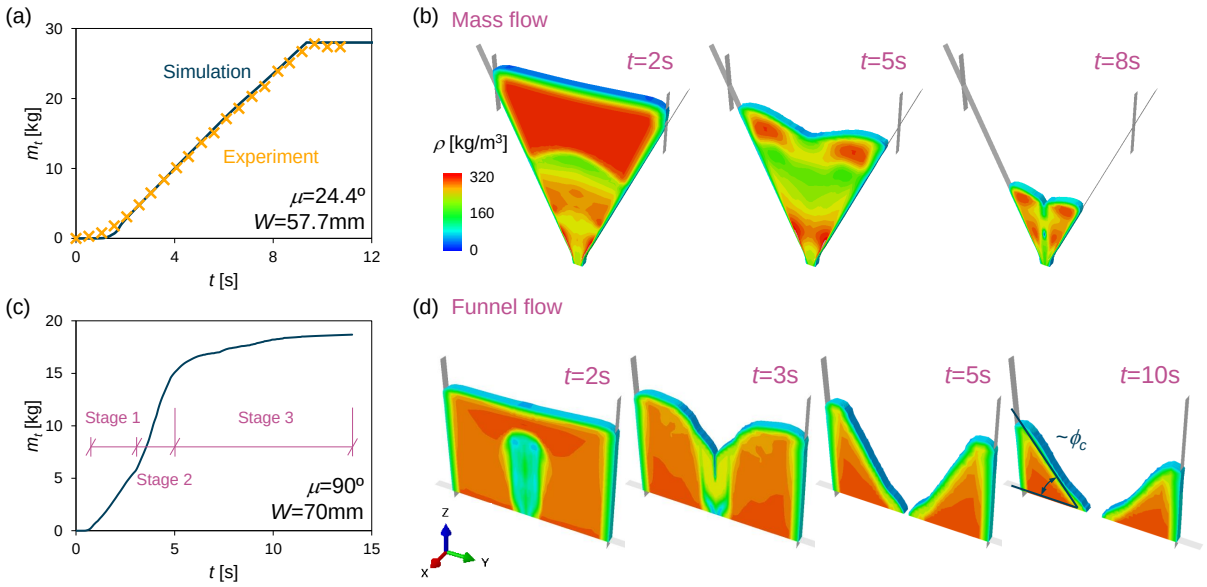

Figure 3: Numerical model validation and predicted flow response for a hopper (low inclination angle) and a silo (high inclination angle). (a) Comparison of simulation predicted cumulative mass discharged m_t against experimental measurements for outlet width $W = 57.7$ mm and hopper inclination $\mu = 24.4°$. (b) Flow pattern demonstration superposed with density distribution for the case in (a). (c-d) Typical flow response of a silo (flat-bottom hopper) with outlet width $W = 70$ mm and inclination $\mu = 90°$.

flow/no-flow conditions. We repeat the open-hold process with the outlet width increased around 1 mm each time, and we stop the process when a steady hopper flow is observed. The critical outlet width W_{cr} is calculated as the average of the outlet widths before and after the steady flow and at the center line (axial direction) of the hopper opening.

Numerical modeling

Reliable modeling of the flow of the highly compressible granular biomass material is challenging for both particle-based methods (e.g., DEM) and continuum mechanics-based methods (e.g., FEM). For DEM, the computational cost and the quantification of the particle-level contact behavior limit its application.[33] For FEM, mesh tangling is difficult to handle for large deformation, and high-fidelity constitutive models across flow regimes do not exist yet.[15,16] The constitutive models (e.g., the classical Mohr-Coulomb model) used for hopper flow simulation in literature[23,34–36] cannot capture the compaction (respectively, dilation)

Table 1: Calibrated G-B hypoplastic model parameters for the pine sample.

ϕ_c [°]	h_s [kPa]	n [-]	e_{d0} [-]	e_{c0} [-]	e_{i0} [-]	α [-]	β [-]
47.3	187.6	0.30	0.50	1.06	1.38	0.3	1.0

induced hardening (respectively, softening) exhibited by the loblolly pine chips. Our recent work on the modeling of granular biomass material flow using an advanced FEM (i.e., the Coupled Eulerian-Lagrangian (CEL) approach), and the Gudehus-Bauer hypoplastic model[37,38] shows the above limitations can be circumvented with promising results.[11] The CEL approach constitutes two steps: 1) a Lagrangian mesh is attached to the material and it deforms with the material using the conventional FEM; 2) the mesh is returned to its original position (i.e., fixed mesh in a whole increment) and the deformed material with its properties are interpolated back onto the "fixed" mesh. This two-step scheme enables CEL capable of modeling large-deformation flow simulations. The G-B hypoplastic model incorporates critical state theory and utilizes void ratio to characterize the density-dependent flow behavior. With these features, we continue using the CEL approach and the G-B model for simulating the complex flow behavior of compressible biomass materials in this study.

The formulation, implementation and validation of the G-B hypoplastic model in Abaqus User Material Subroutine (VUMAT) is described in our previous study[11] and open-sourced in Github. We also proposed a workflow to calibrate the G-B model parameters for ground loblolly pine by combining lab characterization experiments and numerical simulations. Briefly, the eight parameters in the G-B hypoplastic model are: 1) the minimum, the critical, and the maximum void ratios at zero pressure e_{d0}, e_{c0} and e_{i0}, 2) the granulate hardness h_s, exponent n and β, which closely relate to material compressibility, and 3) the internal friction angle at the critical state ϕ_c and exponent α, which determine the shear stress at the critical and the peak states, respectively. The calibrated material parameters are listed in Table 1.

Fig. 2(c) shows the cross-section of the CEL numerical model. Its geometry is exactly the

same as the experimental set-up with fixed bin width as 0.6 m. Similar to the experiments, the hopper outlet width W is adjusted by sliding the hopper wall. A plane strain condition is observed in the experiments with the axis direction perpendicular to the 2D surface shown in Fig. 2(c). Given both the geometry and the boundary conditions are symmetric with respect to the central surface of the two hopper walls, we only simulate a half slice of the cross-section with a finite thickness of 25 mm for the sake of computational efficiency. Except for the walls, we apply symmetric boundary conditions to the planes with normal direction out-of-the-plane and to the symmetric central surface. The hopper walls and the bin are modeled as rigid bodies, with a "hard contact" using the penalty method in the normal direction and a Coulomb frictional contact in the tangential direction. Experimentally determined friction angle 8.5° between the wall and the pine chips is used for all the simulations. We use a structured hexahedron mesh with an average size of 15 mm within the hopper cross-section plane and 5 mm in the axial direction. Constrained by the mesh size (i.e., large mesh distortion and computation efficiency), the time step of 2-20 μs is used for all simulations. We model the experiments using two steps: 1) after the Eulerian meshes are charged with material, we apply the gravity with a smooth step function followed by rest until the internal stress of the material reaches equilibrium, 2) we initiate the flow by sliding the hopper wall from the closing state to the preset outlet width W.

Similar to the experiments, we quantify the mass flow rate q_m and the critical outlet width W_{cr} for each simulation. For the mass flow rate q_m, we extract the nodal velocity and the elemental density for all the outlet elements. Through integration over the outlet surface and time, we plot the predicted accumulative mass discharged against time shown in (Fig. 3(a)). The computed average mass flow rate q_m is the slope of the $m_t - t$ line. For the critical outlet width W_{cr}, we use the Dichotomy method by trying two different outlet widths W and gradually narrowing the range of upper and lower bounds until a dramatic change of flow responses is observed with 2 approaching outlet widths (e.g., $W = 20$ mm and 21 mm in Fig. 4). We also present another method to obtain W_{cr}. After the simulated

mass flow rates against different outlet widths are plotted, we extrapolate the data points $(q_m - W)$ with a line, and denote the intersection point across the line and the horizontal axis as the W_{cr}. The validity of the second method is approved as its predicted W_{cr} is almost the same as the value directly simulated through the Dichotomy method. Details on this method are presented in the *Hopper outlet width* Section.

Model validation

We validate the numerical model by comparing the model predicted cumulative discharged mass m_t against the experimental measurements, as shown in Fig. 3(a) with a hopper inclination angle 24.4° and an outlet width 57.7 mm. In addition, we performed a series of simulations to obtain the mass flow rate q_m variation with different outlet width W at hopper inclination angles 24.4°, 30° and 36°. The match between the numerical prediction and the experimental measurements for all these cases (*Hopper outlet width*) validates the numerical model. It is worth noting that the numerical model developed in this study significantly outperforms the one in our previous study,[11] which realizes the opening of the hopper through the Eulerain boundary condition instead of sliding the walls.

Results

Flow response

Fig. 3(a) and (c) respectively present the modeling predicted variation of cumulative discharged mass m_t against time t for a slender hopper with $\mu = 24.4°, W = 57.7$ mm and a flat-bottom hopper with $\mu = 90°, W = 70$ mm. For most of the hoppers with low inclination angle (we denote them as slender hoppers), the predicted $m_t - t$ flow response is a straight line, which implies the hopper flow is in a steady state and the mass flow rate is a constant. We use the overall flow section in $m_t - t$ response to calculate the slope as the mass flow rate

q_m. The corresponding remaining material at time $t = 2$ s, 5 s, 8 s superposed with density are shown in Fig. 3(b). Recall we use a relatively small wall friction angle (i.e., a smooth wall), the predicted flow has a typical *mass flow* pattern: material at the same height tends to move simultaneously at a similar velocity.

For the flat-bottom hopper (also called silo), a typical *funnel flow* pattern is observed: material above the outlet tends to flow out first and a vertical flow channel is formed as shown in Fig. 3(d). The predicted $m_t - t$ response is not a straight line, and it can be divided into 3 stages (Fig. 3(c)): 1) the material right above the outlet drops out ($t = 2$ s in Fig. 3(d)); 2) the material near funnel surfaces starts to collapse and flow towards the outlet, the overall material height gradually decreases in this stage ($t = 3$ s in Fig. 3(d)); 3) the toes of the funnel surfaces touch the outlet and the flow rate q_m dramatically decreases ($t = 5$ s in Fig. 3(d)), less and less material flow out of the outlet until it fully stops with residual material retained within the silo ($t = 10$ s in Fig. 3(d)). According to the observation, we calculate the mass flow rate q_m from the slope of the Stage 2 $m_t - t$ response. After the material fully stops flowing, we measure the angle between the surface of the residual material and the bottom surface of the silo. We found this angle fluctuates around the critical state internal friction angle ϕ_c. The physical mechanism of the residual material formation inside the silo (i.e., internal material friction) is the same as the formation of the pile for the angle of repose experiment. Note the magnitude of the angle of repose is around ϕ_c.[39,40] The agreement between the residual material slope angle and the critical state internal friction angle further validates the numerical model.

Arching

As described in the *Numerical modeling* Section, the critical outlet width W_{cr} is obtained by the Dichotomy method. Fig. 4(a) shows the variation of cumulative discharged mass with time for the hopper with a fixed inclination $\mu = 24.4^\circ$ and three different outlet widths $W = 19, 20, 21$ mm. For the cases of $W = 19$ and 20 mm, almost zero flow rates are

predicted. While for the case of $W = 21$ mm, we observe a large flow rate. This indicates the W_{cr} around 20.5 mm with a ± 0.5 error bound. Note that the continuum mechanics-based model cannot predict a complete stop of material (Fig. 4(a)). Yet, the almost zero value of the mass flow rate indicates arching is realized.

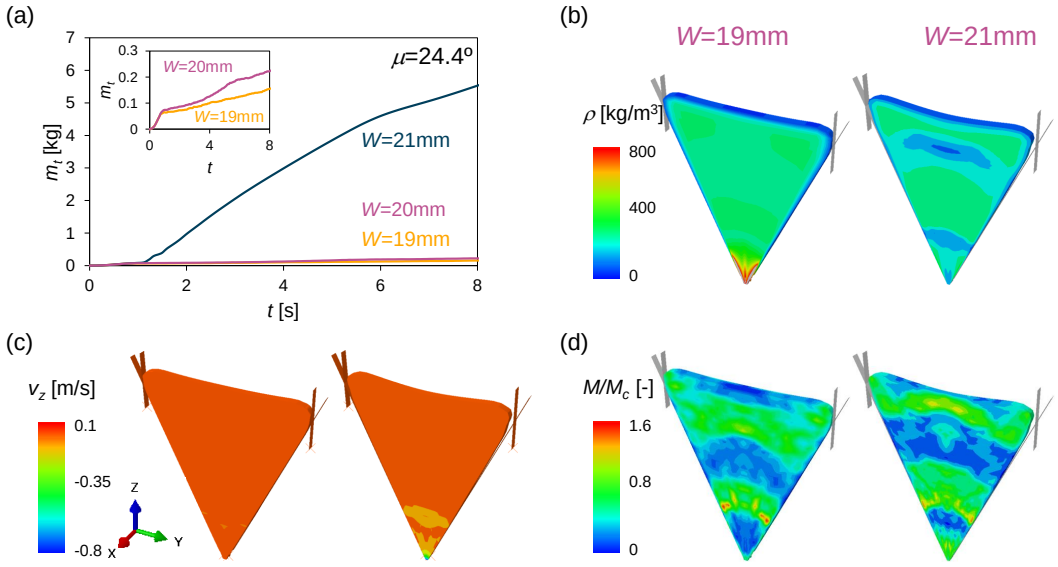

Figure 4: Numerical demonstration of hopper arching. (a) The predicted cumulative mass discharged m_t against time for a hopper with fixed inclination $\mu = 24.4°$ and three outlet width $W = 19, 20, 21$ mm. Free flowing is predicted for $W = 21$ mm while hopper arching is realized for $W = 19, 20$ mm. Note the continuum mechanics-based model cannot model the complete stop of material flow as shown in the small zoomed-in figure, yet, the over one magnitude of difference in predicted flow rate indicates material arching is realized. (b-d) Comparison of the contours of the density (b), the vertical velocity (c), and the normalized friction ratio (d) between the arching hopper case with $W = 19$ mm and the free-flow hopper case with $W = 21$ mm.

We further compare the predicted density ρ, vertical velocity v_z, and normalized friction ratio M/M_c (Fig. 4(b-d)) for the hoppers with $W = 19$ and 21 mm at time $t = 8$ s. Fig. 4(b) shows that the material in the arching hopper ($W = 19$ mm) consolidate and form a high-density region near the outlet, while in the free-flow hopper ($W = 21$ mm), material flow out and a loose region is formed near the outlet. Note the predicted high density shows the limitation of the numeral model, yet, it does not impair the results discussed in this paper. In addition to the density, the near zero vertical velocity v_z predicted for the case of $W = 19$

mm in Fig. 4(c) also indicates material arching.

Fig. 4(d) demonstrates the comparison of the normalized friction ratio M/M_c, where M is defined as the ratio of the deviatoric stress q over the mean stress p, and M_c is the slope of the critical state line in the $q-p$ space. Note M_c is dependent on the Lode angle and the void ratio. This friction ratio M/M_c physically represents whether shear stress is large enough to overcome the confining pressure and to initiate the flow. It is another good indicator of flow/no-flow state and can be interpreted for all critical state-based constitutive model as:

$$M/M_c \begin{cases} \geq 1 & \text{free-flow - material in the critical state,} \\ < 1 & \text{no-flow - material not yet reach the critical state.} \end{cases}$$

According to this theory, the M/M_c near the outlet is much smaller than 1 indicating hopper arching for the case of $W = 19$ mm. But for the case of $W = 21$ mm, the M/M_c near the outlet is close to 1 implying material flow. Note that the small blue band in the $W = 21$ mm hopper case near the outlet is the result of a high void ratio (i.e., low density shown in Fig. 4(b)).

Analyses and discussion

Hopper outlet width

The effect of the hopper outlet width W on the mass flow rate q_m is investigated both numerically and experimentally. Hopper flow tests with the variation of outlet width at the fixed inclination angle of 24.4°, 30°, and 36° were performed. Note we used the same weight of pine chips for all experiments ($\sim$ 28 kg), which results in a slight change in material height within the hopper due to the inclination angle variation. The measured mass flow rates are presented as the yellow '×'s in Fig. 5. Following steps detailed in the *Numerical modeling* Section, the simulation predicted mass flow rates are obtained and shown as the fills

diamonds. We find the numerical prediction can be fitted well with a linear relation shown as the dashed line. These lines closely overlay with the experimental data for all tested hopper inclination angles, demonstrating that increasing outlet width linearly increases the mass flow rate for hopper flow of pine chips. We also find the intersections of the fitted lines with the outlet width W axis, which numerically represent the outlet width at a zero flow rate, overlap with the critical outlet widths W_{cr}^{d} (marked as filled triangles) obtained from the Dichotomy method (*Numerical modeling*). This mutual validation of the Dichotomy and the extrapolating methods demonstrate the robustness of the numerical model.

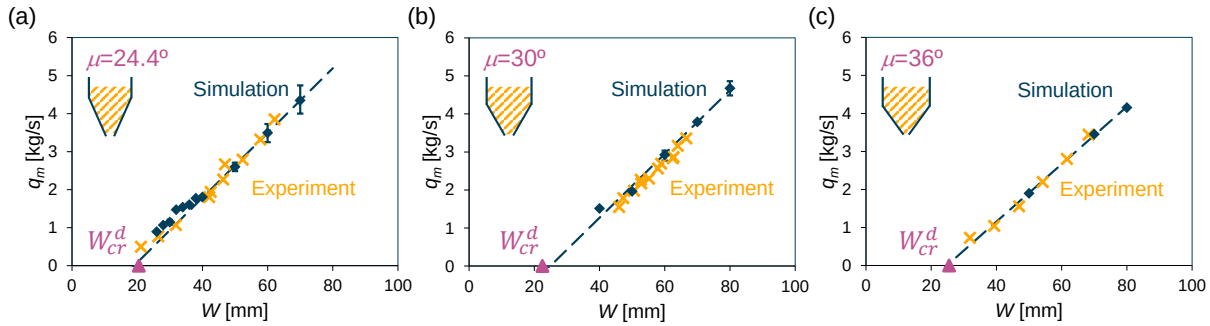

Figure 5: Effect of hopper outlet width W on the mass flow rate q_m with hopper inclination angle of (a) 24.4°, (b) 30° and (c) 36°. For each case, the yellow '×'s stand for experimental measurements, the filled diamonds represent numerical predictions, and the dashed line is fitted from numerical results. The filled triangles located on the W-axes W_{cr}^{d} are the critical outlet widths obtained from the Dichotomy method for each hopper inclination case.

Hopper inclination

Hopper inclination angle is one of the most important design parameters, we study its effect on the mass flow rate q_m and the critical outlet width W_{cr}. Fig. 6(a) presents the comparison of experimental measurements (markers) and numerical predictions (lines) of the $q_m - W$ relationship of the hopper at different inclination angles ($24.4° - 36°$). We observe the numerical predictions have a good match against the experimental measurements, and both of them show the mass flow rate decreases with increasing inclination angle for all fixed outlet widths. This decreasing trend gradually slows down until it reaches a basin around $\mu = 30°$.

For cases with inclination angle exceeds this critical value (i.e., $\mu > 30°$), experimental and numerical data overlap with each other at any given outlet width. The results imply the mass flow rate can be controlled sightly using the inclination angle at a value smaller than the critical one.

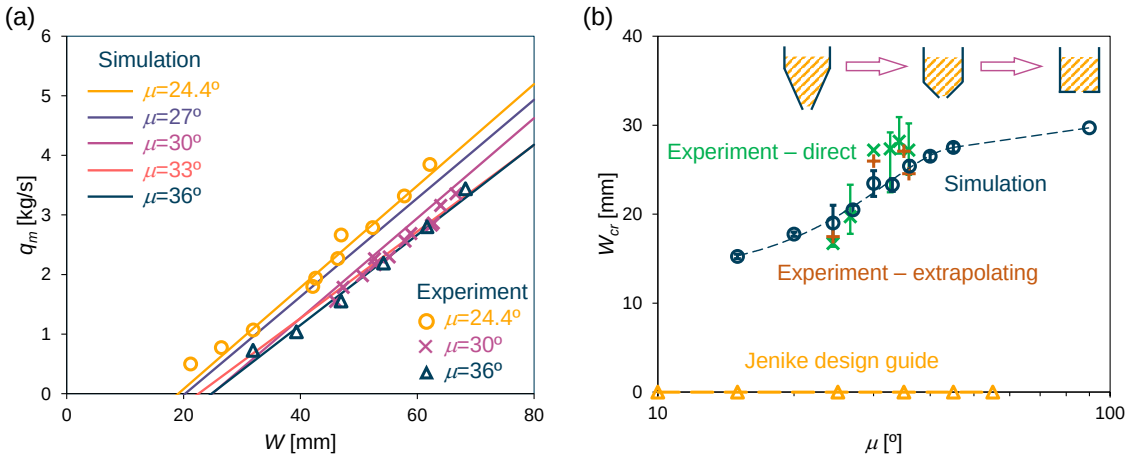

Figure 6: Effect of the hopper inclination angle μ on the mass flow rate q_m and the critical outlet width W_{cr}. (a) The plot of the mass flow rate q_m against the hopper outlet width W at different inclination angle μ. Markers represent experimental measurements, and lines stand for simulation predicted results. Different hopper inclination angles μ are color-coded. (b) The influence of hopper inclination angle μ on the critical outlet width W_{cr}. The green '×'s with error bars are measurements from experiments. The brown '+'s are extrapolated as the intersections of the experiments measured $q_m - W$ fitting lines (Fig. 6(a)) and the W-axis. The dark circles represent numerically obtained W_{cr} from the Dichotomy method and the extrapolating method, note the two methods obtained W_{cr} are close to each other. The yellow triangles are calculated from the classic Jenike design guide. The axis of inclination angle is in log-scale.

Fig. 6(b) presents the variation of the critical outlet width W_{cr} against the hopper inclination angle μ, where yellow triangles are calculated from the classic Jenike design guidline, green '×'s are experimentally measured results using the Dichotomy method described in the *Experimental setup* Section, brown '+'s are obtained as the intersections between the fitting lines of the experiments measured $q_m - W$ data and the W axis as described in the *Hopper outlet width* Section, and the dark circles stand for numerically obtained W_{cr} from both the Dichotomy method and the extrapolating method. Note that the numerical predictions of W_{cr} from the two methods are almost identical, which gives negligible error bars for each

case. With these data points, we conclude the numerical and experimental results generally agree with each other. The small difference is due to the local effect of pine samples near the outlet area with a non-representative particle size distribution. This localization effect is often observed in biorefineries as a variation of critical outlet size is observed for the same feeding material. In contrast to the numerical and experimental results, the Jenike design approach[17,18] predicts no arching for all the cases. This over-estimation of the material flowability clearly explains the inconsistent flow experienced by many biorefinaries.

In general, both the numerical predictions and the experimental measurements show the critical outlet width W_{cr} increases with the increasing hopper inclination angle. When μ is small, the flow is initiated first as the gravity ($F_g = \sqrt{F_s^2 + F_n^2}$) induced driven force F_s along the wall exceeds the wall friction resistance $F_n \tan \phi_w$, recall a low wall friction angle $\phi_w = 8.5^\circ$ is used for experiments and simulations. When the inclination angle μ increases, gravity results in more normal force ($F_n = \sin \mu F_g$) and less driven force ($F_s = \cos \mu F_g$), so that an increasing outlet width is needed to flow the material. When μ becomes large enough, overcoming the friction resistance within the material is more easier comparing to overcoming the wall friction resistance. Material shear along a plane with an inclination angle μ' smaller than μ, and funnel flow pattern occurs.

Initial packing

Time effect (i.e., material consolidation) is another important reason for biomass handling issues in biorefineries. For conventional granular materials, their particles are almost non-compressible, consolidation is negligible in the time period of material storage and handling. Yet, the high compressibility of biomass particles results in compaction during the consolidation under self-weight. In this section, we investigate the time effect by simulating hopper discharge with a fixed mass of materials (30 kg) at different initial packing conditions. This varying initial compaction is realized by assign different values of the initial density/void ratio. As demonstrated in Fig. 7(b), a high void ratio or a low density corresponds to a loose

packing, and a low void ratio or a high density stands for dense packing.

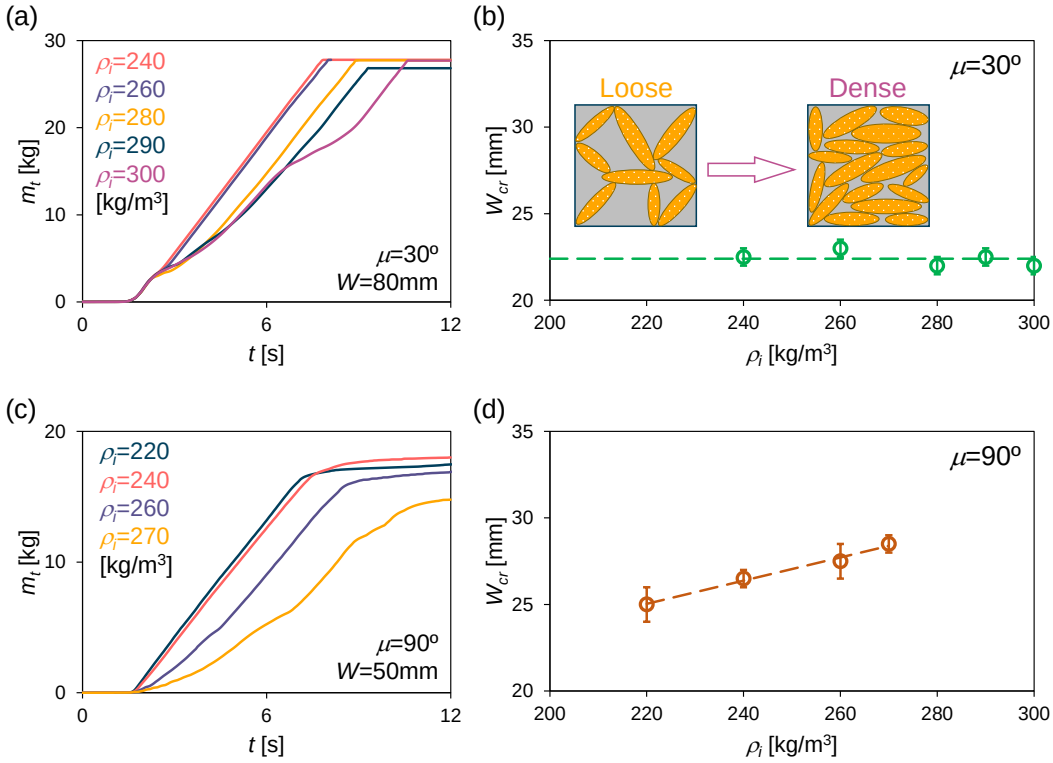

Figure 7: Effect of the initial packing on the mass flow rate q_m and the critical outlet width W_{cr}. (a, c) Predicted cumulative discharged mass m_t versus time t for a slender hopper with $\mu = 30°$ and a flat-bottom hopper with $\mu = 90°$, respectively. (b, d) Predicted critical outlet width W_{cr} at different initial packing conditions ρ_i in the slender hopper and in the flat-bottom hopper.

Fig. 7 demonstrates the influence of initial packing on the flow behavior and the critical outlet width W_{cr}. Fig. 7(a) and (c) show the variation of the cumulative discharged mass m_t against time in a slender hopper with $\mu = 30°$ and a flat-bottom hopper with $\mu = 90°$, respectively. In both plots, we find the cases with loose packing initially (e.g., $\rho_i = 220 - 240$ kg/m^3) result in straight and smooth flow responses. For the cases with dense packing initially (e.g., $\rho_i = 300$ kg/m^3 in Fig. 7(a) and 270 kg/m^3 in Fig. 7(c)), the slope of $m_t - t$ response varies from time to time, implying a surging or chunk-by-chunk flow behavior is predicted. Surging flow not only results in inconsistent material feeding, but also creates dynamic loading on the handling equipment. The influence of initial packing on the critical outlet width W_{cr} is shown in Fig. 7(b) and (d). For the slender hopper, we observe that W_{cr}

is not sensitive to the initial packing condition. However, the increase of W_{cr} with increasing initial density ρ_i indicates flow initiation gets harder for a densely packed material in the flat-bottom hopper.

The physical mechanism of these predicted flow behavior is the dilation (respectively, compaction) requirement of densely (respectively, loosely) packed material for flow. According to the critical state theory, material flow only occurs when both the stress and void ratio reach their corresponding critical state value. Given all materials within the hopper are assigned with the same packing density, the dilation of densely packed material away from the outlet requires extra space. This requirement can only be satisfied when the material below flows out and makes the way for volume expansion. This process occurs chunk-by-chunk manifested as surging flow (Fig. 7(a, c)). For loosely packed material, it is compacted throughout the whole hopper while flowing, which results in smooth flow behavior. For critical outlet width W_{cr}, the balance between the driven force and the resistance near the outlet determines its value. For the slender hopper, the wall friction angle determines the two forces as explained in the *Hopper inclination* Section, and the value of W_{cr} is not sensitive with packing (Fig. 7(b)). However, for the flat-bottom hopper, the internal friction angle at the critical state determines the balance of the two forces. A densely packed material requires a higher driving force than a loosely packed material to reach the balance, which results in a higher magnitude of the critical outlet width (Fig. 7(d)).

Particle density variability

One distinctive feature of granular biomass materials in comparison with conventional granular materials is their multi-scale variability.[41,42] For ground loblolly pine, the most important variability is the particle density ρ_p given the critical state theory uses void ratio as a state variable that needs to be calculated via particle density. Direct measurement of ρ_p is challenging because of the existence of inner pores within particles and the difficulty to distinguish the inner pores from the exterior pores (void space among particles).[31] Usually,

Table 2: G-B-hypoplastic model parameters for the pine samples with different particle density.

ρ_p [kg/m^3]	ϕ_c [°]	h_s [kPa]	n [-]	e_{d0} [-]	e_{c0} [-]	e_{i0} [-]	α [-]	β [-]
350	47.3	55.0	0.327	0.17	0.68	0.88	0.32	1.7
400	47.3	129.0	0.304	0.38	0.92	1.19	0.30	1.2
430	47.3	187.6	0.300	0.50	1.06	1.38	0.3	1.0
500	47.3	354.9	0.285	0.77	1.40	1.82	0.27	0.8
550	47.3	494.0	0.280	0.96	1.64	2.13	0.26	0.6

the particle density is estimated from the density of the original wood block. However, the density of wood can be different among tree plantation location,[43] tree age and height,[44] and position of the wood on each tree. Therefore, we investigate the influences of particle density variability on the hopper flow performance.

The variation of particle density is not straightforward for the G-B hypoplastic model, instead, it is embedded within all the constitutive parameters. After selecting a reasonable range of the particle density for pine chips around 430 kg/m^3, which is the value we have used so far, we calibrate the model parameters according to the same workflow reported in our previous work[11] against the same set of experimental data. The calibrated constitutive parameters with different ρ_p are listed in Table 2. With these parameters, we perform hopper flow simulations to obtain the flow response and the critical outlet width W_{cr}. Results are summarized in Fig. 8. Note that the range of particle density is selected based on previous studies.[31,43,44] Table 2 shows the most sensitive parameters to the particle density variability ρ_p is the granulate hardness h_s, it increases almost one-magnitude for a change of ρ_p from 350 to 550 kg/m^3. Other parameters are either not dependent on ρ_p (ϕ_c), or not sensitive (α, β, n). Note that the void ratios (e_{d0}, e_{c0}, e_{i0}) serve as the bounding limits of the constitutive model and monotonously increase with increasing ρ_p.

Fig. 8(a) and (c) present the numerically obtained mass flow rate q_m variation with hopper outlet width W in a slender hopper of $\mu = 30°$ and a flat-bottom hopper of $\mu = 90°$, respectively. We observe that particle density does not have a significant influence on the

mass flow rate. Note we only show the two cases with the minimum and maximum particle densities given all other cases have similar results.

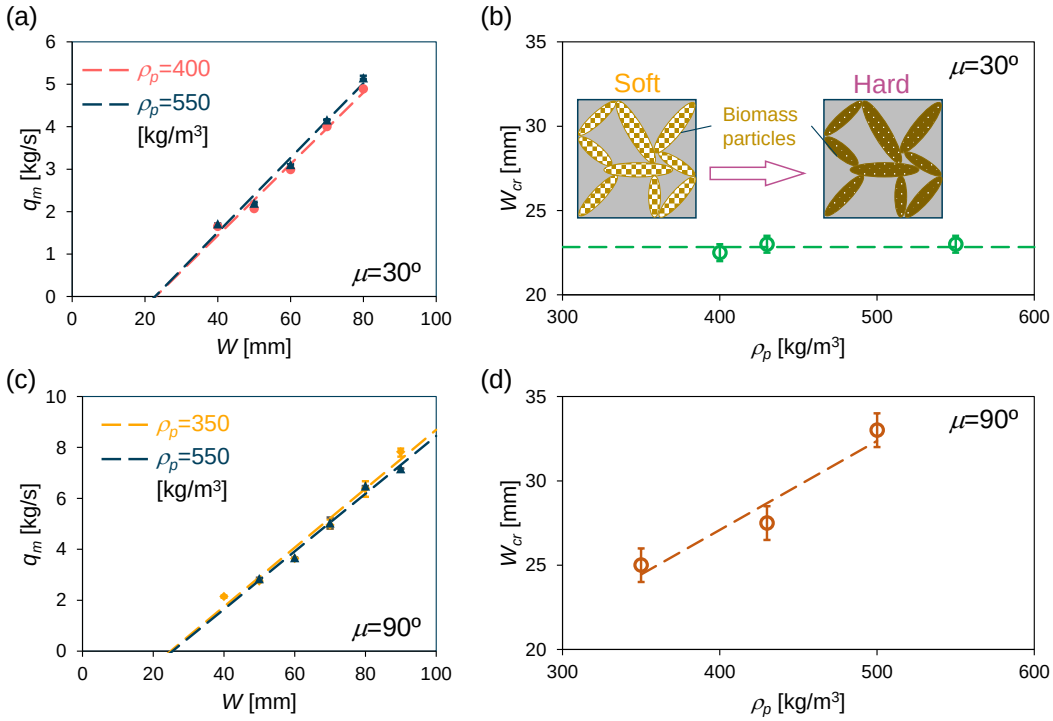

Figure 8: Effect of particle density variability on flow performance. (a, c) Predicted mass flow rate q_m of pine chips with different particle density against hopper outlet width W for a slender hopper ($\mu = 30°$) and a flat-bottom hopper ($\mu = 90°$). (b, d) The critical outlet width W_{cr} predicted at different particle density ρ_p for hoppers with inclination angle of 30° and 90°.

Different from the mass flow rate, the predicted critical outlet width W_{cr} for the flat-bottom hopper ($\mu = 90°$) changes significantly with particle density (Fig. 8(d)). This dependence is not observed for the slender hopper ($\mu = 30°$, Fig. 8(b)). As sketched in Fig. 8(b), a low particle density stands for soft particles, while a high ρ_p represents hard particles. Under the same loading condition, the material with a high granulate stiffness undergoes smaller deformation and interlocks more easily comparing to the material with a low granulate stiffness. This poor flowability with interlocking happens within the material. For the slender hopper, the critical balance of driven force and resistance is located at the wall as explained before, W_{cr} is independent of the interlocking induced by hard granulate stiffness. However, for the flat-bottom hopper, internal friction and interlocking within the material

determine the balance of the driven force and resistance. Consequently, the material with a higher granulate stiffness requires more driving force to counterbalance the interlocking, and a higher critical outlet width has resulted.

Surcharge

The surcharge, such as applying dead weight on the top of the feedstock in the hopper or filling more material, is a practice adopted to facilitate hopper discharge. The underline mechanism of surcharge is to add additional vertical stress as the driving force for hopper flow, however, the success of this practice varies case by case. Limited investigations have been done in literature on the influence of surcharge on the flow performance and the critical outlet width. In this section, we study the surcharge effect through filling height variation by numerically simulating the discharge process of the hopper filled with different amounts of material. Similar to the previous sections, we performed two sets of simulations with a slender hopper ($\mu = 24.4°$) and a flat-bottom hopper ($\mu = 90°$).

Fig. 9(a) presents the cumulative discharged mass m_t with time for different initial amount of material in a slender hopper ($\mu = 24.4°$ and $W = 70$ mm). Note the case with $M = 22.2$ kg corresponds to a hopper without an upper bin, its $m_t - t$ is a straight line. For the other two cases, the $m_t - t$ responses are dual-linear. By observing the flow process, we find the dual-linear response has resulted from the two-stage flow behavior. In the first stage, the material is discharged under the vertical pressure of the upper-bin material, and this stage ends when the top surface of the material touches the hopper-bin intersection. In the second stage, the rest of the material inside the hopper flows out without any surcharge. The two-stage flow process is verified by the equivalent mass flow rate of the 2^{nd} stage for all cases shown in Fig. 9(b). Contrary to the assumption that surcharge can facilitate hopper flow, we observe mass flow rate decrease with increasing filling height (reflected as the total amount of mass M) for the 1^{st} stage (Fig. 9(b)). We further examine this finding by modeling hopper flow with different outlet widths. Fig. 9(c) plots the predicted q_m against hopper

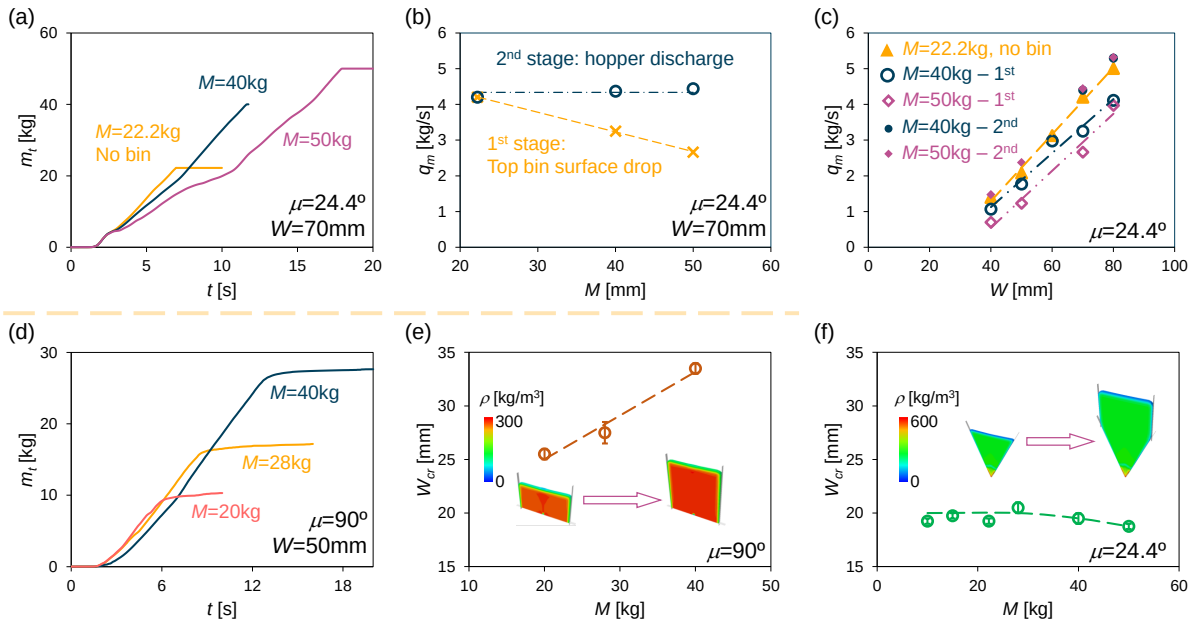

Figure 9: Effect of filling height on the flow response. (a, d) Predicted cumulative discharged mass m_t against time with different initial amount of materials for a slender hopper ($\mu = 24.4°$ and $W = 70$ mm) and a flat-bottom hopper ($\mu = 90°$ and $W = 50$ mm). Two stages of the flow rate (i.e., the slope of the $m_t - t$ response) are observed for the slender hopper (a). Note the case with material mass $M = 22.2$ kg does not have enough material inside the upper bin, only a straight line is predicted for $m_t - t$. (b) The mass flow rate q_m variation with the initial amount of material M obtained from the two stages. (c) Mass flow rate q_m variation against hopper outlet width W for different initial amounts of material and different stages. (e, f) The critical outlet width W_{cr} predicted for the flat-bottom hopper and the slender hopper against the initial filled material mass M.

outlet width W for different initial filling mass M. It is clear that the mass flow rate of the 2^{nd} stage overlap with each other and the mass flow rate decreases with increasing initial filling material mass for all cases. This phenomenon is also observed for the flat-bottom hopper as shown in Fig. 9(d). The critical outlet width W_{cr} affected by the total amount of material is shown in Fig. 9(e-f). In the flat-bottom hopper, the initiation of flow becomes harder with a heavier surcharge (Fig. 9(e)). However, for the slender hopper (Fig. 9(f)), the W_{cr} keeps constant when M is small, and it starts to decrease when M exceeds 22.2 kg.

The above phenomena of flow performance result from two competing mechanisms as we increase the surcharge: 1) the extra weight of material compacts the material inside the hopper and decreases material flowability; 2) the extra weight of material increases

the discharge driven force and facilitates the flow. The compaction mechanism is clearly demonstrated in Fig. 9(a-d), the mass flow rate decreases with increasing surcharge weight for both the slender hopper and the flat-bottom hopper. The facilitation mechanism is reflected in the critical outlet width for the slender hopper case. Significant portion of surcharge weight is added to the flow driving force $F_s = \cos\mu F_g$ with small μ, and the critical outlet width W_{cr} decrease with increasing M when $M > 22.2$ kg as shown in Fig. 9(f). For $M < 22.2$ kg, the material's height does not reach the hopper-bin intersection, the added weight is balanced by the wall friction resistance, which results in constant critical outlet width. Note the compaction mechanism has insignificant influence on critical outlet width in slender hoppers as detailed in the *Initial packing* Section. For the flat-bottom hopper, the material stagnation zone creates a shear surface with a high inclination angle, less portion of the surcharge weight is used to drive material flow. In addition, the high internal friction angle increases the resistance. The combination of a less driving force and more resistance results in a trivial effect for flow facilitation of the surcharge weight. The compaction mechanism dominates this case, wider outlet opening is needed for more initial filling material.

We conclude the surcharge has significant influences on the hopper flow performance, which is contradictory to the literature.[23,35] We argue that: 1) the material (pine chips) used in this study has much higher compressibility than the conventional granular materials (e.g., sand),[11] compaction is more significant; 2) the constitutive model, used in previous studies (e.g., Mohr-Coulomb model), is not capable of capturing density-dependent flow behavior, while the G-B hypoplastic model used in this study can. These discrepancies demonstrate the significance of using a density/void ratio dependent model to characterize the flow behavior of compressible biomass materials.

Conclusions

Biomass material is a promising and sustainable energy resource but is limited in use because of significant difficulties and financial losses on material handling. In this work, we focus on a representative biomass material, loblolly pine chips, and investigate its flow performance in a wedge-shaped hopper. We first designed a wedge-shaped hopper at the pilot-scale with adjustable wall inclination angle and outlet width. We then experimentally studied the hopper flow rate response and the critical hopper outlet width at various combinations of hopper inclination and outlet opening width. After a three-dimensional FEM model was developed and validated against the experimental data, we numerically investigated the hopper flow performance affected by the outlet width, hopper inclination, initial packing, biomass particle density, and the filling height. Main contributions and conclusions are summarized as follows:

1. The numerical model consisting of the G-B constitutive law and the CEL solver is a reliable tool to study hopper flow performance. A combination of physical experiments and comprehensive simulations is a cost-effective and time-efficient approach to address bulk material flow challenges at all scales.

2. The mass flow rate of pine chips increases with the hopper outlet width linearly, and it decreases with the wall inclination angle slightly. The decreasing trend stops when the inclination angle reaches the critical value of around 30°. The initiation of the flow is easier for a slender hopper as the critical outlet width increases with increasing inclination angle.

3. The flow pattern of the compressible particles is closely related to the initial packing of the material. A dense packing results in surging flow while a loose packing has a continuous smooth flow. More dense packing results in a wider critical outlet width for silo (flat-bottom hopper), not for slender hoppers.

4. The variability of biomass particle density creates uncertainty for the calibration of material constitutive parameters. Its influence on hopper flow performance is trivial except the critical outlet width for the silo: higher particle density results in a higher critical outlet width.

5. Surcharge affects the flow performance with two competing mechanisms: flow impedance by the compaction of material and flow facilitation by the increase of discharge driven force. The mass flow rate is dominated by the compaction mechanism so that the mass flow rate decreases with increasing surcharge weight. For the critical outlet width, the compaction mechanism also dominates in silos, higher surcharge weight results in wider critical outlet width. Yet, the facilitation mechanism dominates in slender hoppers.

These findings can help biorefineries to solve a piece of the long-lasting puzzle on flow inconsistency and arching. A comprehensive understanding of the flow behavior of compressible particulate materials considering moisture content and feedstock variability is underway. All these work will be used to construct a novel design method for material handling equipment and to optimize feedstock processing in biorefineries.

Acknowledgement

This work was supported by the U.S. Department of Energy (DOE), Office of Energy Efficiency and Renewable Energy (EERE), Bioenergy Technologies Office (BETO), under DOE Idaho Operations Office Contract DE-AC07-05ID14517. Any opinions, findings and conclusions, or recommendations expressed in this material are those of the authors and do not necessarily reflect those of the DOE or the U.S. Government.

References

1. Carpenter, D.; Westover, T. L.; Czernik, S.; Jablonski, W. Biomass feedstocks for renewable fuel production: a review of the impacts of feedstock and pretreatment on the yield and product distribution of fast pyrolysis bio-oils and vapors. *Green Chemistry* **2014**, *16*, 384–406, DOI: 10.1039/C3GC41631C.

2. Bilgili, F.; Koçak, E.; Bulut, Ü.; Kuşkaya, S. Can biomass energy be an efficient policy tool for sustainable development? *Renewable and Sustainable Energy Reviews* **2017**, *71*, 830–845, DOI: 10.1016/j.rser.2016.12.109.

3. Langholtz, M. H.; Stokes, B. J.; Eaton, L. M. 2016 Billion-ton report: Advancing domestic resources for a thriving bioeconomy, Volume 1: Economic availability of feedstock. *Oak Ridge National Laboratory, Oak Ridge, Tennessee, managed by UT-Battelle, LLC for the US Department of Energy* **2016**, *2016*, 1–411.

4. *Biorefinery Optimization Workshop Summary Report*; 2016.

5. Hess, J. R.; Wright, C. T.; Kenney, K. L. Cellulosic biomass feedstocks and logistics for ethanol production. *Biofuels, Bioproducts and Biorefining: Innovation for a sustainable economy* **2007**, *1*, 181–190, DOI: 10.1002/bbb.26.

6. Dale, B. A sober view of the difficulties in scaling cellulosic biofuels. *Biofuels, Bioproducts and Biorefining* **2017**, *1*, 5–7, DOI: 10.1002/bbb.1745.

7. Ilic, D.; Williams, K.; Farnish, R.; Webb, E.; Liu, G. On the challenges facing the handling of solid biomass feedstocks. *Biofuels, Bioproducts and Biorefining* **2018**, *12*, 187–202, DOI: 10.1002/bbb.1851.

8. Ramírez-Gómez, Á. Research needs on biomass characterization to prevent handling problems and hazards in industry. *Particulate Science and Technology* **2016**, *34*, 432–441, DOI: 10.1080/02726351.2016.1138262.

9. Cheng, Z.; Leal, J. H.; Hartford, C. E.; Carson, J. W.; Donohoe, B. S.; Craig, D. A.; Xia, Y.; Daniel, R. C.; Ajayi, O. O.; Semelsberger, T. A. Flow behavior characterization of biomass feedstocks. *Powder Technology* **2021**, *387*, 156–180, DOI: 10.1016/j.powtec.2021.04.004.

10. Leal, J. H.; Torres, E. L.; Rouse, W. T.; Moore, C. M.; Sutton, A. D.; Hoover, A. N.; Li, C.; Resch, M. G.; Donohoe, B. S.; Ray, A. E., et al. Impacts of Inorganic Material (Total Ash) on Surface Energy, Wettability, and Cohesion of Corn Stover. *ACS Sustainable Chemistry & Engineering* **2020**, *8*, 2061–2072, DOI: 10.1021/acssuschemeng.9b06759.

11. Lu, Y.; Jin, W.; Klinger, J.; Westover, T. L.; Dai, S. Flow characterization of compressible biomass particles using multiscale experiments and a hypoplastic model. *Powder Technology* **2021**, *383*, 396–409, DOI: 10.1016/j.powtec.2021.01.027.

12. Westover, T. L.; Phanphanich, M.; Ryan, J. C. Comprehensive rheological characterization of chopped and ground switchgrass. *Biofuels* **2015**, *6*, 249–260, DOI: 10.1080/17597269.2015.1091189.

13. Hernandez, S.; Westover, T. L.; Matthews, A. C.; Ryan, J. C. B.; Williams, C. L. Feeding properties and behavior of hammer-and knife-milled pine. *Powder technology* **2017**, *320*, 191–201, DOI: 10.1016/j.powtec.2017.07.002.

14. Barletta, D.; Berry, R. J.; Larsson, S. H.; Lestander, T. A.; Poletto, M.; Ramírez-Gómez, Á. Assessment on bulk solids best practice techniques for flow characterization and storage/handling equipment design for biomass materials of different classes. *Fuel Processing Technology* **2015**, *138*, 540–554, DOI: 10.1016/j.fuproc.2015.06.034.

15. Jin, W.; Klinger, J. L.; Westover, T. L.; Huang, H. A density dependent Drucker-Prager/Cap model for ring shear simulation of ground loblolly pine. *Powder Technology* **2020**, *368*, 45–58, DOI: 10.1016/j.powtec.2020.04.038.

16. Jin, W.; Stickel, J. J.; Xia, Y.; Klinger, J. A review of computational models for the flow of milled biomass Part II: Continuum-mechanics models. *ACS Sustainable Chemistry & Engineering* **2020**, *8*, 6157–6172, DOI: 10.1021/acssuschemeng.0c00412.

17. Jenike, A. W. *Gravity flow of bulk solids*; Bulletin of the University of Utah, 1961; Vol. 52.

18. Jenike, A. W. *Storage and flow of solids*; Bulletin of the University of Utah, 1964; Vol. 53.

19. Mehos, G.; Eggleston, M.; Grenier, S.; Malanga, C.; Shrestha, G.; Trautman, T. Designing Hoppers, Bins, and Silos for Reliable Flow. *The Best of Equipment Series* **2018**, 33.

20. Walker, D. A basis for bunker design. *Powder Technology* **1967**, *1*, 228–236, DOI: 10.1016/0032-5910(67)80041-X.

21. Enstad, G. On the theory of arching in mass flow hoppers. *Chemical Engineering Science* **1975**, *30*, 1273–1283, DOI: 10.1016/0009-2509(75)85051-2.

22. Drescher, A.; Waters, A.; Rhoades, C. Arching in hoppers: II. Arching theories and critical outlet size. *Powder Technology* **1995**, *84*, 177–183, DOI: 10.1016/0032-5910(95)02982-8.

23. Pardikar, K.; Wassgren, C. Predicting the critical outlet width of a hopper using a continuum finite element method model. *Powder Technology* **2019**, *356*, 649–660, DOI: 10.1016/j.powtec.2019.08.111.

24. Miccio, F.; Barletta, D.; Poletto, M. Flow properties and arching behavior of biomass particulate solids. *Powder technology* **2013**, *235*, 312–321, DOI: 10.1016/j.powtec.2012.10.047.

25. Guo, J.; Roberts, A. W.; Prigge, J.-D. Experimental investigation of wall pressure and

arching behavior under surcharge pressure in mass-flow hoppers. *Powder technology* **2014**, *258*, 272–284, DOI: 10.1016/j.powtec.2014.03.048.

26. Søgaard, S. V.; Olesen, N. E.; Hirschberg, C.; Madsen, M. H.; Allesø, M.; Garnaes, J.; Rantanen, J. An experimental evaluation of powder flow predictions in small-scale process equipment based on Jenike's hopper design methodology. *Powder Technology* **2017**, *321*, 523–532, DOI: 10.1016/j.powtec.2017.08.006.

27. Xue, J.; Schiano, S.; Zhong, W.; Chen, L.; Wu, C.-Y. Determination of the flow/no-flow transition from a flat bottom hopper. *Powder Technology* **2019**, *358*, 55–61, DOI: 10.1016/j.powtec.2018.08.063.

28. Li, J.; Langston, P. A.; Webb, C.; Dyakowski, T. Flow of sphero-disc particles in rectangular hoppers—a DEM and experimental comparison in 3D. *Chemical Engineering Science* **2004**, *59*, 5917–5929, DOI: 10.1016/j.ces.2004.07.022.

29. Zhao, Y.; Cocco, R. A.; Yang, S.; Chew, J. W. DEM Study on the effect of particle-size distribution on jamming in a 3D conical hopper. *AIChE Journal* **2019**, *65*, 512–519, DOI: 10.1002/aic.16483.

30. Xia, Y.; Chen, F.; Klinger, J. L.; Kane, J. J.; Bhattacharjee, T.; Seifert, R.; Ajayi, O. O.; Chen, Q. Assessment of a tomography-informed polyhedral discrete element modelling approach for complex-shaped granular woody biomass in stress consolidation. *Biosystems Engineering* **2021**, *205*, 187–211, DOI: 10.1016/j.biosystemseng.2021.03.007.

31. Xia, Y.; Lai, Z.; Westover, T.; Klinger, J.; Huang, H.; Chen, Q. Discrete element modeling of deformable pinewood chips in cyclic loading test. *Powder technology* **2019**, *345*, 1–14, DOI: 10.1016/j.powtec.2018.12.072.

32. Wang, Y.; Lu, Y.; Ooi, J. Y. Finite element modelling of wall pressures in a cylindrical silo with conical hopper using an Arbitrary Lagrangian–Eulerian formulation. *Powder Technology* **2014**, *257*, 181–190, DOI: 10.1016/j.powtec.2014.02.051.

33. Xia, Y.; Stickel, J. J.; Jin, W.; Klinger, J. A Review of Computational Models for the Flow of Milled Biomass Part I: Discrete-Particle Models. *ACS Sustainable Chemistry & Engineering* **2020**, *8*, 6142–6156, DOI: 10.1021/acssuschemeng.0c00402.

34. Zheng, Q.; Yu, A. Finite element investigation of the flow and stress patterns in conical hopper during discharge. *Chemical Engineering Science* **2015**, *129*, 49–57, DOI: 10.1016/j.ces.2015.02.022.

35. Zheng, Q.; Xia, B.; Pan, R.; Yu, A. Prediction of mass discharge rate in conical hoppers using elastoplastic model. *Powder technology* **2017**, *307*, 63–72, DOI: 10.1016/j.powtec.2016.11.037.

36. Pardikar, K.; Zahid, S.; Wassgren, C. Quantitative comparison of experimental and Mohr-Coulomb finite element method simulation flow characteristics from quasi two-dimensional flat-bottomed bins. *Powder Technology* **2020**, *367*, 689–702, DOI: 10.1016/j.powtec.2020.04.036.

37. Gudehus, G. A comprehensive constitutive equation for granular materials. *Soils and foundations* **1996**, *36*, 1–12, DOI: 10.3208/sandf.36.1.

38. Bauer, E. Calibration of a comprehensive hypoplastic model for granular materials. *Soils and foundations* **1996**, *36*, 13–26, DOI: 10.3208/sandf.36.13.

39. Herle, I.; Gudehus, G. Determination of parameters of a hypoplastic constitutive model from properties of grain assemblies. *Mechanics of Cohesive-frictional Materials: An International Journal on Experiments, Modelling and Computation of Materials and Structures* **1999**, *4*, 461–486, DOI: 10.1002/(SICI)1099-1484(199909)4:5<461::AID-CFM71>3.0.CO;2-P.

40. Cornforth, D. *Evaluation of relative density and its role in geotechnical projects involving cohesionless soils*; ASTM International, 1973; DOI: 10.1520/STP37878S.

41. Ray, A. E.; Williams, C. L.; Hoover, A. N.; Li, C.; Sale, K. L.; Emerson, R. M.; Klinger, J.; Oksen, E.; Narani, A.; Yan, J., et al. Multiscale Characterization of Lignocellulosic Biomass Variability and Its Implications to Preprocessing and Conversion: a Case Study for Corn Stover. *ACS Sustainable Chemistry & Engineering* **2020**, *8*, 3218–3230, DOI: 10.1021/acssuschemeng.9b06763.

42. Kenney, K. L.; Smith, W. A.; Gresham, G. L.; Westover, T. L. Understanding biomass feedstock variability. *Biofuels* **2013**, *4*, 111–127, DOI: 10.4155/bfs.12.83.

43. Jordan, L.; Clark, A.; Schimleck, L. R.; Hall, D. B.; Daniels, R. F. Regional variation in wood specific gravity of planted loblolly pine in the United States. *Canadian Journal of Forest Research* **2008**, *38*, 698–710, DOI: 10.1139/X07-158.

44. Schultz, R. P. *Loblolly pine: the ecology and culture of the loblolly pine (Pinus taeda L.)*; US Government Printing Office, 1997; pp 26–27.

Synposis We investigate the granular flow mechanisms of milled-biomass particles to tackle the material handling challenges experienced by the bio-energy industry.

TOC/Abstract Graphic

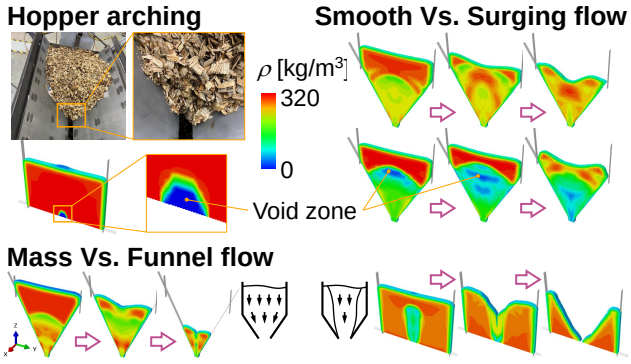

Revision 1 - Response to Reviewers for **sc-2021-05628s**

Flow and arching of biomass particles in wedge-shaped hoppers

by Yimin Lu, Wencheng Jin, Jordan Klinger, and Sheng Dai.

We thank the three anonymous reviewers and the editor for their valuable inputs on our manuscript. Below, we respond in detail to each of the reviewers' comments.

Reviewer: 1

Through an integrated numerical and experimental approach, the authors investigate the flow characteristics and arching of biomass particles (pine chips) in wedge-shaped hoppers. The predictions of G-B hypoplastic model are validated against experimental findings. The effect of hopper outlet width, hopper inclination, initial packing, particle density variability, and surcharge is comprehensively investigated and discussed throughout the manuscript. The topic of the research is novel and the paper is very well written and organized. The results are valuable to the community. Therefore, I recommend the publication of paper. A few minor comments are given below:

Thank you for the encouraging comments. Please see the responses below.

Comments

- Page 3 lines 36-39: appropriate reference(s) missing

  Thanks, we added the relevant references in the revised manuscript.

- Page 8 lines 141-146: It is rather confusing to list eight G-B hypoplastic model parameter under three categories.

  The categorization of constitutive parameters according to their physical meanings is intended to help the readers form a clear view on the parameters. In addition, the three categories also fall in the three characterization experiments used for calibration: void ratios (category 1) are obtained from index tests, compressibility related three parameters (category 2) are calibrated against oedometer tests, and the shear related two parameters (category 3) are calibrated from Schulze ring shear test. Please see our previous publication (Lu., et. al (2021). Flow characterization of compressible biomass particles using multiscale experiments and a hypoplastic model. Powder Technology, 383, 396-409.) for details, and we hope this addresses your confusion.

Reviewer: 2

Comments

- The authors should review the paper one more time to improve the grammar and fix a few spelling mistakes.

  Thanks, we revised the manuscript according to the great comments of reviewers and we proofread the manuscript thoroughly.

- Please provide additional detail on the implementation of the continuum model, perhaps in an appendix. For example, discuss the mesh characteristics, time step, etc.

  The details of the continuum model (i.e., the CEL solver, the hypoplastic constitutive law, and the boundary value problem-hopper flow) was detailed in our previous publication (Lu., et. al (2021). Flow characterization of compressible biomass particles using multiscale experiments and a hypoplastic model. Powder Technology, 383, 396-409.). Except the hopper opening (static v.s. dynamic) is modeled differently and explained in the manuscript, we used the same continuum model in this effort. With tools established in our previous effort, we focus more on the physical interpretation of the prediction against experimental observations in this paper.
  For the sake of completeness, we added a few details on the mesh and time steps in the revised manuscript following your suggestion. Specifically, we performed a sensitivity analysis to evaluate the effects of mesh and time step with the implemented hypoplastic model. The nature of the two-step computational scheme of CEL requires an intermediate mesh size and a corresponding range of time steps, otherwise, details are lost for a coarse mesh or computational cost is non-affordable for a fine mesh. The influence of time step on the predicted results is negligible, and increasing mesh size slightly decreases the mass flow rate. An average mesh size of 15mm in the hopper cross-section plane and 5mm in the axial direction is used for all the simulations given it provides the best match with experimental results.

- I recommend that the point you make in Fig. 4 about how the continuum model cannot predict the complete stop in the material flow should be discussed in the main text too. It's easy to overlook in the figure caption. A little additional discussion of this point would be helpful.

  Thanks for the suggestion. We added the corresponding details in the main text.

- It appears in Fig. 4 that the material pulls away from the hopper walls near the junction with the upper bin. Please explain why that occurs. Does it have any impact on the predictions?

  Thanks for noting this nonphysical presentation. This is caused by the CEL numerical method and the post-processing techniques for display, and it has no impacts on the predictions. To overcome the mesh entangling issue in conventional FEM flow simulations, this study uses the Coupled Eulerian-Lagrangian (CEL) FEM. The CEL approach uses an Eulerian "fixed" mesh with material flows through it and tracked by the volume fraction in each element. As a results, if an element is not fully occupied

by the material, its volume fraction is less then 1. The post-process requires a cut-off of the volume fraction to show the material boundary. With the value we chosen, a few elements at the the hopper-bin junction area with volume fraction below the cut-off value was not shown with material, which leads to the impression of material pulls away from the wall.

- The authors should compare their mass flow rate vs. width findings (proportional to width) with the widely-reported slot mass flow rate behavior (proportional to width raised to the 1.5 power), including the Rose and Tanaka correlation for inclined hopper walls. For example, see Dhodapkar, S., Jacob, K., and Kodak, M., 2016, "Determining discharge rates of particulate solids", Chemical Engineering Progress, Vol. 112, pp. 50 - 61. Do you have any insight as to why there would be this scaling discrepancy?

  Thanks for the great comment. We believe you are referring the mass flow rate estimation from the British Materials Handling Board:

$$q_m = 1.03\rho_b\sqrt{g}(L - kd)(W - kd)^{1.5}F$$

  where ρ_b is the bulk density, g is the gravity, L and W are the hopper depth (axial direction) and outlet width, k is a particle shape parameter and is suggested as 2.5 for non-spherical particle, d is the mean particle size, F is the hopper inclination parameter and $F = (\tan\mu)^{-0.35}$ where μ is the hopper inclination angle.

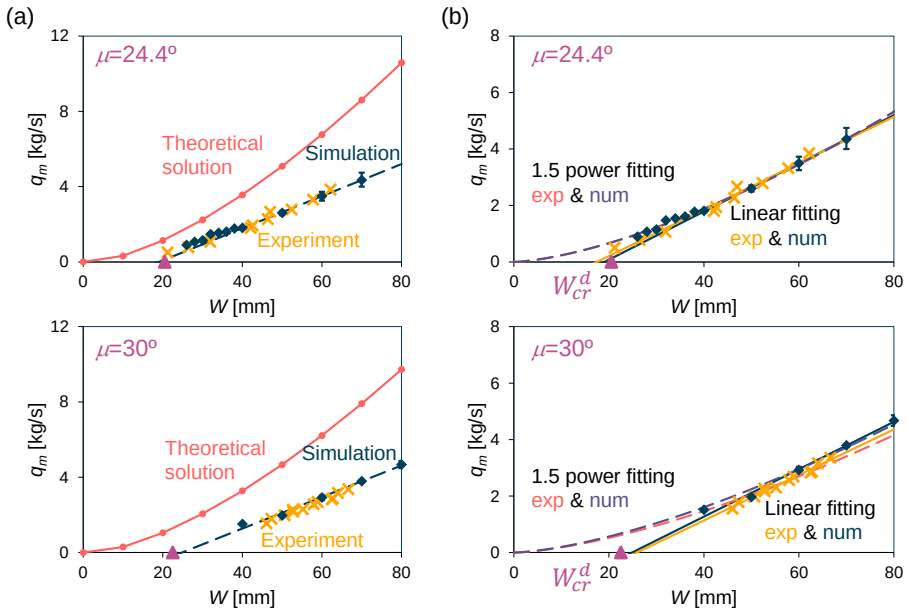

(a) Theoretical predicted mass flow rate with $\mu = 24°$ and 30° plotted with experimental measurements and numerical predictions. (b) Data fitting with both linear and 1.5-power relationships.

The equation-predicted q_m with $\mu = 24°$ and 30° are plotted against the experimental measurements and the numerical predictions in Fig. **??***(a). We find the equation*

R-square of fitting relationships.

	$\mu = 24.4°$ exp.	$\mu = 30°$ exp.	$\mu = 24.4°$ num.	$\mu = 30°$ num.
Linear	0.9791	0.9801	0.9940	0.9889
1.5-power	0.9654	0.9442	0.9962	0.9836

significantly overestimates the mass flow rate. We believe the unique features of compressible pine chips, especially the large internal friction angle, the high compressibility and the high particle aspect ratio, cause the discrepancy. In addition, this equation also significantly underestimates the critical outlet width $W_{cr} = kd$.
By adjusting the coefficient in the equation, we can fit a 1.5-power relationships to the experimental and numerical results as shown in Fig. **??***(b). Qualitatively, both linear and power relationships have a satisfied agreement with the q_m data, but only the linear trend can explain the critical outlet width at the intersection. Quantitatively, the calculated R-square of linear fitting line is better in comparison to the R-square of power fitting line as list them Table* **??***.*
We admit above reasoning is only valid for the range of hopper outlet width we tested. Both physical experiments and numerical simulations needs to be carried out to test whether the power law or linear relationship is better in predicting the mass flow rate outside this range.

- The authors should compare their measured and simulated critical exit widths with predictions from the classic Jenike approach. I realize that there are experimental challenges with obtaining the required Jenike parameters, but this comparison would be very much of interest to the readers. Just how far off are the Jenike predictions from what you've measured?

  Agreed. The comparison will be a good demonstration of the incompetence of classical design guide on compressible biomass materials. We added the prediction from Jenike approach in Fig. 6 and added corresponding description in the text.

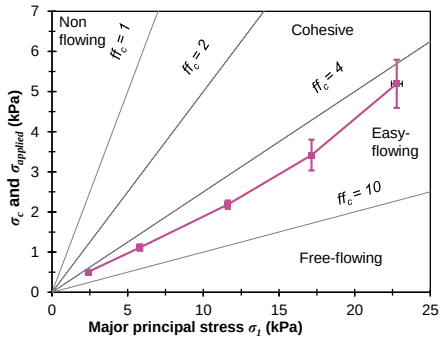

Flow function of the material used in this study.

As shown in the figure, the flow function of the tested material always falls in the easy-

flowing range (the inverse of the flow factor always greater than 4), which indicates the Jenike approach predicts zero critical outlet width for all the cases.

- To help explain the results in Fig. 9, it would be useful to show density field plots of the hoppers with different surcharges.

  We appreciate the suggestion. We replaced the sketch of hoppers with density field plots.

Reviewer 3

This work studies the flow and arching of wood chips in hoppers. The bulk handling of biomass-type material is indeed important in practices as such materials differ largely from traditional bulk sands or ores, in terms of particle shape, density and so on. This paper uses both an experiment and a novel hypoplastic model to systematically investigate the arching problem, which I think is remarkable. Only two minor issues may be noticed.

We appreciate the supportive comments. Please see the responses below.

Comments

- The hypoplastic model and CEL simulation are not described in details. The theoretical background of the model is important for the readers to evaluate the effectiveness of the results.

  We agree with reviewer that the model theory is an important aspect to convince readers on the effectiveness of results. Given the constraint of words limit, we only added a few sentences in the revised manuscript on the model features to illustrate why the numerical model is capable of simulating compressible biomass material flow. As explained in the response of reviewer-2's question 2, we also cited our previous work (Lu., et. al (2021). Flow characterization of compressible biomass particles using multiscale experiments and a hypoplastic model. Powder Technology, 383, 396-409.), which details the theory on the hypoplastic model and the CEL approach. With tool development established before, the current manuscript emphasizes using the developed tool to understand the flow and arching physics.

- Page 23, LN 415, the authors found that the surcharge has a significant influence on hopper performance. Is it a experimental observation or a numerical result? How large is the surcharge pressure? Can the hypoplastic model give a reasonable modelling of such phenomenon. Thanks

  The effect of surcharge is numerically studied, and the surcharge pressure for the simulations in this section is about 3 kPa.
  We believe the flow models with the hypoplastic law in this study can realistically capture the surcharge phenomenon given:

  1. *The G-B hypoplastic model is based on the critical-state-theory and can capture the density-dependent behavior. This implies that the model not only can capture the increasing vertical stress caused by surcharge (like what other constitutive laws can do), but it also can predict the surcharge-induced compaction. For example, we have shown the model can simulated the high compressibility of pine chips in our previous study (Lu., et. al (2021)).*
  2. *The hypoplastic material parameters are calibrated in our previous study (Lu., et. al (2021)), in which the shear behavior predicted numerically agrees well with the experimental data with the maximum surcharge of 10 kPa. This range well covers the surcharge magnitude in the hopper flow simulations (3 kPa).*